Crumpled Nitrogen-Doped Graphene for Supercapacitors with High Gravimetric and Volumetric Performances

Jie Wang, Bing Ding, Yunling Xu, Laifa Shen, Hui Dou, and Xiaogang Zhang*

Jiangsu Key Laboratory of Materials and Technology for Energy Conversion, College of Material Science and Engineering, Nanjing University of Aeronautics and Astronautics, Nanjing, 210016, P. R. China

S Supporting Information

ABSTRACT: Graphene is considered a promising electrochemical capacitors electrode material due to its high surface area and high electrical conductivity. However, restacking interactions between graphene nanosheets significantly decrease the ion-accessible surface area and impede electronic and ionic transfer. This would, in turn, severely hinder the realization of high energy density. Herein, we report a strategy for preparation of few-layer graphene material with abundant crumples and high-level nitrogen doping. The two-dimensional graphene nanosheets (CNG) feature high ion-available surface area, excellent electronic and ion transfer properties, and high

packing density, permitting the CNG electrode to exhibit excellent electrochemical performance. In ionic liquid electrolyte, the CNG electrode exhibits gravimetric and volumetric capacitances of 128 F g^{-1} and 98 F cm^{-3}, respectively, achieving gravimetric and volumetric energy densities of 56 Wh kg^{-1} and 43 Wh L^{-1}. The preparation strategy described here provides a new approach for developing a graphene-based supercapacitor with high gravimetric and volumetric energy densities.

KEYWORDS: supercapacitor, graphene, confinement carbonization, electrochemistry, volumetric performance
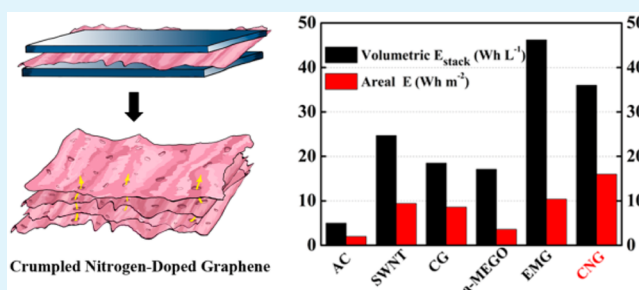
INTRODUCTION

Electrochemical capacitors (ECs), also known as supercapacitors, represent an attractive kind of energy storage devices. Typically, ECs have received wide attention because of their superior cycling durability and high power density. However, the real application was restricted by its relatively low energy density.[1−5] To generate a high energy-storage density, significant research has been directed to the preparation of novel electrode materials that could combine long cycle life and high power output along with high energy density.[6−11] Graphene has recently gained extensive attention as a promising EC electrode material, owing to its high theoretical specific surface area (SSA, ∼2630 m^2 g^{-1}), excellent electroconductivity, and low packing density.[12−15] However, because of the strong van der Waals attraction between parallel graphene sheets, the aggregation or restacking of graphene is unavoidable and would greatly diminish the ionic-accessible surface area, thus decreasing the specific capacitance. Furthermore, the horizontal alignment of the stacked graphene would hinder electron and ion transfer, especially at high rate charge and during the discharge process.[16−19] To mitigate these problems, considerable efforts have been directed to developing porous graphene-based electrodes with high electrolyte accessibility, including (1) the manipulation of individual graphene sheet morphology, such as "crumpled" or "curved" sheets, resulting in a more open structure around each layer and higher effective surface area;[20−22] (2) the chemical functionalization of graphene to manipulate physical and chemical

properties of graphene, such as nitrogen (N),[20,23−25] boron (B),[26] and sulfur (S)[27,28] modification; and (3) the insertion of molecular or nanostructured spacer materials into graphene sheets to increase the interlayer spacing.[29,30] All of these methods could improve the contact between electrolyte ions and surface of graphene, leading to a high specific capacitance. However, facile preparation of graphene material with high ion-available surface area and rapid electronic and ionic transfer is still a challenge.

Although capacitance per weight (C_m) was traditionally used as an important parameter for estimating the electrochemical performance of electrode materials, the capacitance per volume (C_v) is becoming increasingly essential for energy-storage devices with limited space.[4,31−36] However, for most electrode materials, the gravimetric and volumetric capacitances (C_m and C_V, respectively) are generally in a trade-off relationship. Porous materials with high surface area usually shows a low packing density (ρ), leading to a low C_V ($C_m = \rho C_V$).[4,33] A high-density electrode may promote the volumetric performance relatively. However, the electrolyte-available surface area was greatly reduced, and the ion transport path was blocked, thus sacrificing the C_m and rate capability.[37] Recent work reported by Li's group has shown a kind of porous yet densely packed graphene film through capillary compression in the presence of
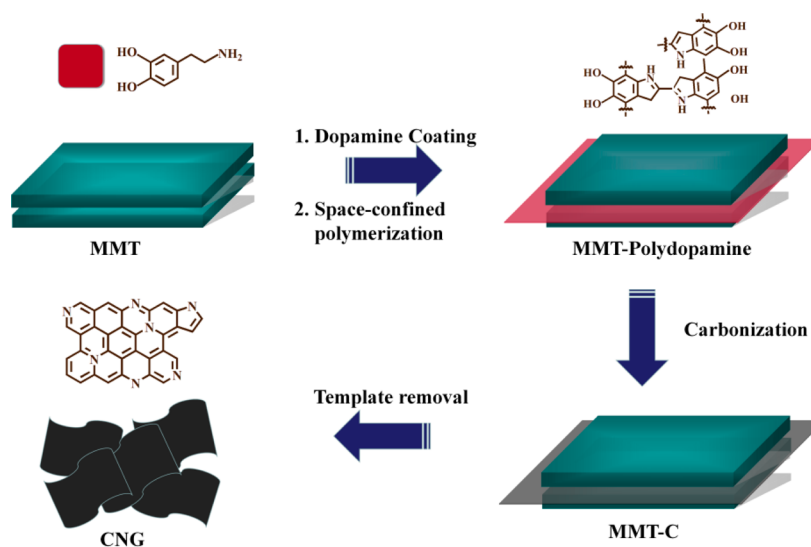
Figure 1. Schematic illustration of CNG synthesized through confined-carbonization strategy.
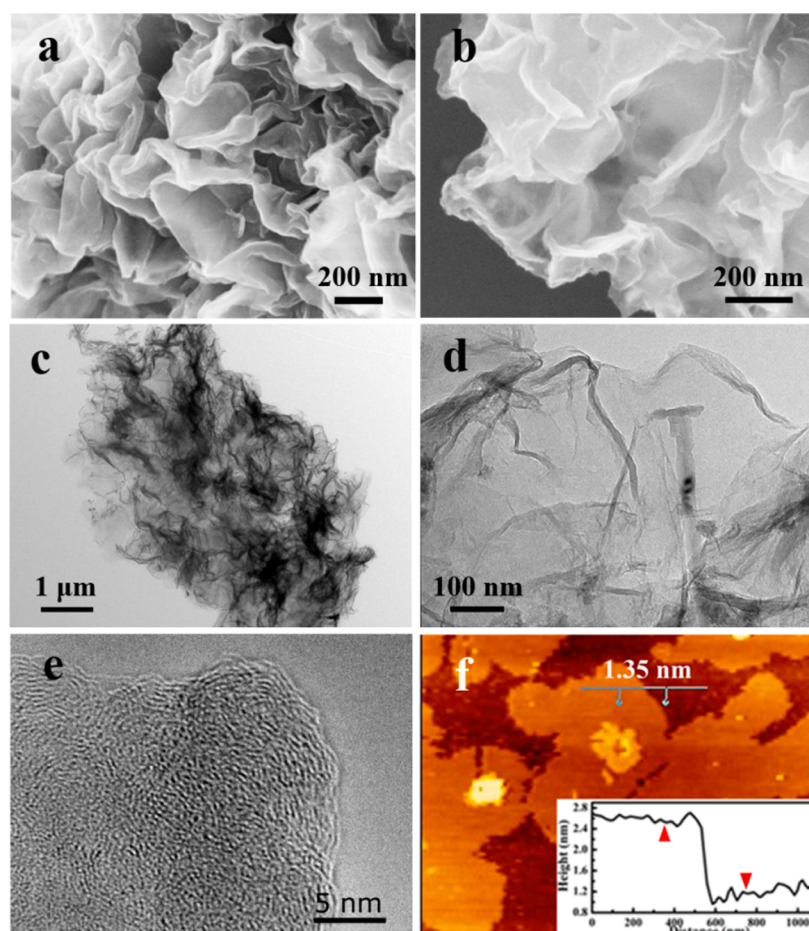

Figure 2. SEM (a,b), TEM (c,d) and HRTEM (e) images of CNG; AFM image of CNG with height profile (f).

electrolyte; the electrolyte-mediated graphene electrode created a continuous ion diffusion network, approaching extremely high C_v and volumetric energy density (E_v) values.[32] Actually, the surface property and geometric structure show significant effects on the high-level charge propagation at the interface of the electrode material. Hence, to fabricate supercapacitors achieving outstanding gravimetric as well as volumetric

performance, investigations should be focused on high-density graphene materials but with suitable porous structure and good wettability, which could provide the maximum real surface available for electrolyte.

Herein, we develop a new strategy for preparing highly crumpled and nitrogen-doped graphene (CNG) for EC electrodes. The facile ion-transport pathway and high packing
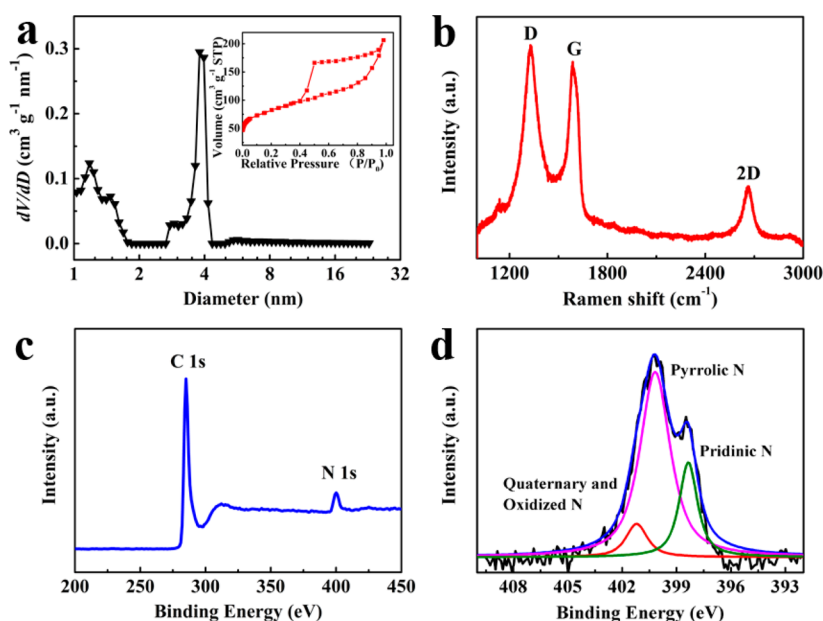
Figure 3. PSD and N_2 sorption isotherms (inset) of the CNG (a); Raman spectrum of the CNG (b); XPS survey spectrum (c) and deconvoluted N 1s spectrum (d) of the CNG.

density enable this two-dimensional (2D) CNG electrode simultaneously with high C_m and C_v of 128 F g^{-1} and 98 F cm^{-3} in ionic liquid. Furthermore, the CNG symmetric supercapacitor also delivers a high E_v of 43 Wh L^{-1}. More inspiringly, devices made with CNG are less independent of the loading level of the active material, meaning that scalable devices can be possibly achieved with our CNG material.

RESULTS AND DISCUSSION

The synthesis procedure of the CNG is schematically presented in Figure 1. In the first step, a nitrogen-rich carbon precursor (dopamine; DA) was added into a montmorillonite (MMT) aqueous dispersion until they are well- blended. DA was introduced to the interlayer of MMT and then was allowed to polymerize within the confined nanospace. The polymer/MMT nanocomposite was then carbonized in N_2 to convert the polydopamine (PDA) into carbon, followed by the etching of the template to obtain N-doped crumpled graphene. MMT, as a unique template, could be used to prepare graphenelike carbon material, and the graphitizability is independent of the precursor.[38] Furthermore, when using a nitrogen-rich carbon precursor, MMT can exclude quaternary N and enable more planar pyridinic and pyrrolic N during carbonization.[39,40] The preparation procedure of CNG was tracked by X-ray diffraction (XRD). As shown in Figure S1, no peaks of MMT were detected in the final product, suggesting the complete removal of the template from the sample. Meanwhile, the (002) and (100) reflections at approximately $2\theta = 25°$ and $44°$ are due to a graphitic phase in CNG.[41]

The morphology and nanostructure of the as-prepared CNG were characterized through electron microscope images. The scanning electron microscopy (SEM) images display a spacious 2D geometry of CNG (Figure 2a,b). There are abundant wavy folds on the surface of graphene sheets, which creates many nanosized voids uniformly distributed inside and between the films. Such unique nanostructure, on the one hand, could help resist the restacking of overlapped graphene and serve as an ion-buffering region. On the other hand, the pocketlike districts

in graphene sheets can shorten the ion transport distance and accelerate ionic flow and electron transport during charge and discharge process (Figure S2). Transmission electron microscopy (TEM) images (Figure 2c,d) further confirm the crumpled 2D structure created by MMT templates. Furthermore, the (002) graphitic basal planes, as revealed in the high-resolution TEM (HRTEM) images, indicate the graphitic structure within CNG (Figure 2e).[42] Atomic force microscopy (AFM) was carried out to investigate the thickness of CNG. As shown in Figure 2f, CNG is about 1−1.5 nm in thickness, which is only about 3−6 graphitic layers.[28]

The N_2 sorption isotherms of the CNG display a type IV curve with a H2 hysteresis loop, which can be attributed to the presence of mesopores (Figure 3a).[43] The SSA of CNG is about 401 m^2 g^{-1}, which is comparable with chemically reduced graphene oxide materials. The pore size distribution (PSD) curve reveals that the pore sizes of CNG are mainly distributed around 3.3 and 1.2 nm. On the one hand, the large numbers of crumples on the CNG contribute to the abundant mesopores. On the other hand, during the decomposition of PDA, a large amount of gas is released, thus forming dense micropores. The Raman spectra of CNG shows a feature of a few-layer graphene (Figure 3b). The CNG shows a G band at 1587 cm^{-1} accompanied by an obvious 2D peak at 2650 cm^{-1}, suggesting that it was a mixture of 2−4 layer graphene. The sharp D band clearly indicates the existence of defects generated by micropores and nitrogen doping in the graphene layer.[44] As revealed in Figure 3c, the N-doping of CNG was further verified by X-ray photoelectron spectroscopy (XPS) spectra. The high-resolution C 1s spectrum can be deconvoluted to three component peaks, assigning to sp^2 C−sp^2 C (284.9 eV), N−sp^2 C (285.5 eV), and N−sp^3 C (286.5 eV) bonds, respectively (Figure S3).[45] The N 1s spectrum can also be deconvoluted to three subpeaks (Figure 3d). These three subpeaks are attributed to the pyridinic (399.1 eV), pyrrolic (401.2 eV), and graphitic types (402.7 eV) of N atoms doped in the graphene structure, respectively.[46] It should be noted that the percentage of active pyrrolic and pyridinic N atoms is
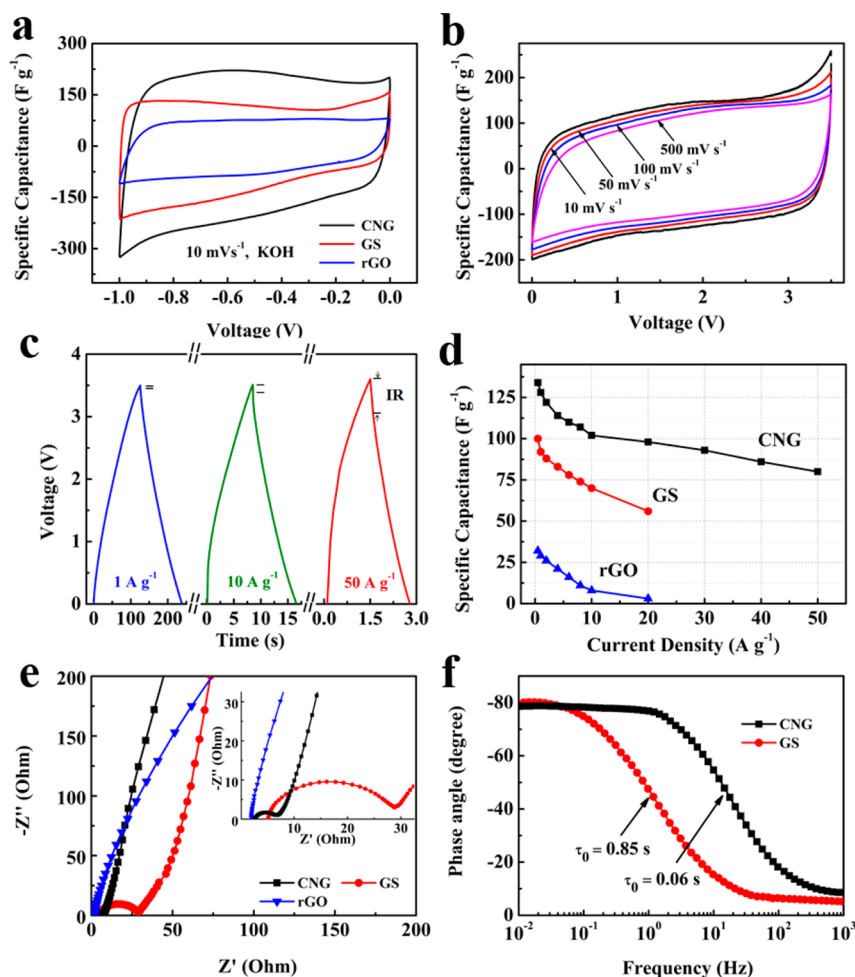
Figure 4. CV plots of different electrodes in a three-electrode system with 6 M KOH electrolyte (a); CV plots of CNG-based symmetric supercapacitors in EMImBF$_4$ electrolyte (b); GCD curves of CNG supercapacitor (c); specific capacitances of different graphene-based supercapacitors at various current densities in EMImBF$_4$ electrolyte (d); Nyquist plots (e) and frequency response of the phase angle (f) of different electrodes.

much higher than that of graphitic-type N. This phenomenon demonstrates that N is incorporated in planar sp^2 hybridization, verifying the confinement effect of the flat nanoreactor.[39] Element-mapping images were carried out to analyze the elemental carbon and nitrogen distributions in CNG. The uniform distribution of colorful spots indicates the homogeneous doping of N in CNG (Figure S4).

The highly crumpled structure with hierarchically porous nanostructure of CNG enables its potential as electrode materials for high-performance ECs. Cyclic voltammetry (CV) plots of CNG, GS, and chemically reduced graphene (rGO) samples measured in a three-electrode system are compared in Figure 4a. The first difference concerns the shape of the voltammograms. The typical rectangular shape in the case of GS and rGO can be observed, while CNG material shows a wide reversible hump, suggesting that the capacitance comes from EDLC and pseudocapacitance together. In addition, the CNG electrode exhibits highest capacitance. Notwithstanding the fact that CNG and GS present comparable SSA and similar PSD patterns (Figure S5), the higher capacitance of CNG is mainly related to an additional pseudofaradaic contribution.[47] Such electrochemical performances suggest the promising potential applications of CNG materials as supercapacitor electrode.

To better investigate the supercapacitive performances of CNG, we further measured it in a two-electrode configuration in ionic liquid electrolyte. As shown in Figure 4b, the CV curve of CNG-based supercapacitor in EMImBF$_4$ electrolyte can still remain a rectangular shape on increasing the scan rate up to 500 mV s^{-1}. Meanwhile, the galvanostatic charge and discharge (GCD) curve in Figure 4c showed a nearly symmetric triangular shape with a small voltage drop (0.8 V) at 50 A g^{-1}, indicating a relatively low equivalent series resistance (ESR) value of 8 Ω. CV and GCD results that both suggest an ideal electric double-layer capacitive behavior and rapid ionic and electric transport throughout the CNG electrode. Contrary to the results of the three-electrode system, CV curves of symmetric system show no obvious humps contributed by redox reaction. With large electrolyte-available surface area and an excellent ion-diffusion property, the CNG exhibits the highest capacitances among all samples at various current densities (Figure 4d). For instance, the CNG electrode shows a specific capacitance of 128 F g^{-1} at a current density of 1 A g^{-1}. It is much higher than the specific capacitance for rGO and GS, which are 52 and 107 F g^{-1}, respectively. It is noted that even at a current density of 50 A g^{-1}, the CNG electrode continues to provide 81 F g^{-1}, corresponding to capacitance retention of 63%. These values demonstrate that the CNG electrode not
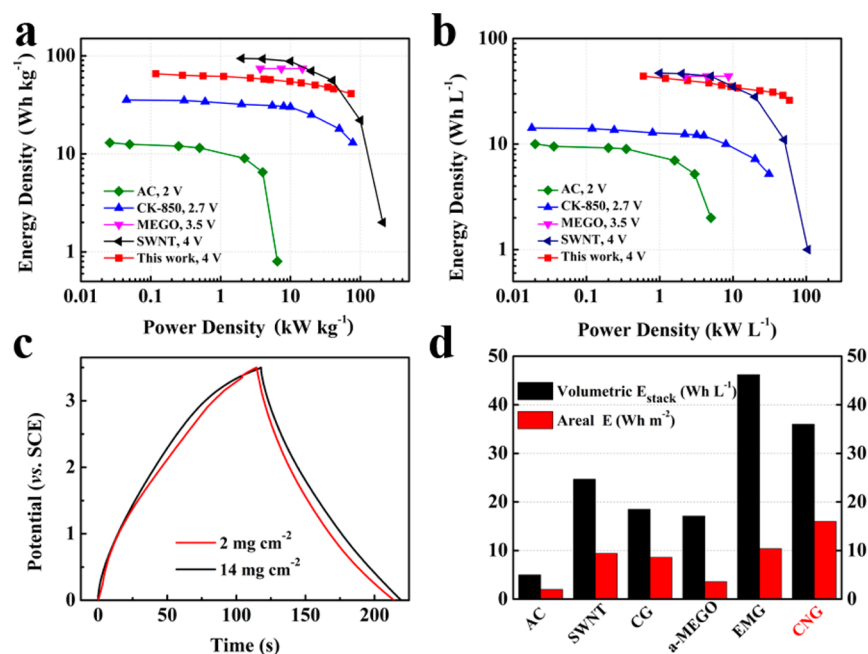
Figure 5. Gravimetric (a) and volumetric (b) performances of the CNG compared with previous reports: AC (ref 49), SWNT (ref 50), CK-850 (ref 52), MEGO (ref 53). GCD curves of CNG supercapacitor with different mass loading (c). Volumetric stack energy densities and areal energy densities for ECs made from various carbon materials: AC (ref 49), SWNT (ref 50), CG (ref 19), a-MEGO (ref 54), and EMG (ref 32) (d). Reproduced with permissions from ref 32. Copyright 2013 AAAS, ref 49. Copyright 2007 Elsevier, ref 50. Copyright 2010 John Wiley and Sons, ref 54. Copyright 2011 AAAS.

only shows high specific capacitance but also exhibits improved rate capability at ultrafast charge and discharge rate. Because CNG and GS have similar porous structures, we propose that the different behavior, especially at high current density, could be due to their different surface chemistry. The nitrogen functional groups on the CNG surface may facilitate the wetting of the IL electrolyte on the electrodes, which then increased the accessible surface area. To prove the improved wettability of CNG electrode, we performed a contact-angle test with IL electrolyte. The results show that the electrolyte–carbon contact angle is ∼20° (versus 69° for GS), demonstrating a more hydrophilic surface allowing the wetting of previously inaccessible pores (Figure S6).

The Nyquist plot of the CNG electrode consists of a small diameter semicircle, a short 45° district, and a straight line in the low-frequency regime, further confirming the nearly ideal capacitive behavior and faster ion diffusion in the CNG electrode. As shown in Figure 4e, the CNG electrode exhibits an ESR value with 8 Ω, which is in accordance with the results of GCD test. The ESR value is a combination of intrinsic resistance of the CNG materials and resistance in charge separation at electrode and electrolyte interface.[37] Albeit the higher conductivity of rGO than CNG (∼1400 versus ∼1100 S m^{-1}), the smallest ESR value of CNG features its more efficient ion-diffusion path from the electrolyte to the surface of the electrode material. The highly accessible surface area of CNG to the electronic double layer formation is also characterized by an exceptionally small relaxation time constant τ_0 of 0.06 s (Figure 4f), which is much lower than that of the GS-based device (τ_0 = 0.85 s) or the EM-CCG film-based device (τ_0 = 0.51 s).[32,48] The cycle stability of CNG was measured through GCD test at a high current density of 4 A g^{-1}, as shown in Figure S7. The CNG electrode retained more than 91% capacitance over 100 000 cycles. This result clearly indicates the

excellent electrochemical stability and reversibility of CNG materials.

Figure 5a,b show the Ragone plot of the CNG-based symmetric supercapacitors. The maximum energy density of the CNG/CNG symmetric supercapacitor is up to 56 Wh kg^{-1}, surpassing most other carbon-based symmetric supercapacitors.[49−53] This is particularly relevant in that the cell still retains an energy density of 37 Wh kg^{-1} at 62 kW kg^{-1}, suggesting that the sample affords the release of lots of energy in a short time. Because the mass density of active materials is about 0.76 g cm^{-3}, it can be reckoned that the maximum C_V of CNG in ionic liquid electrolyte is up to 98 F cm^{-3}. Correspondingly, the maximum E_V was calculated to be 43 Wh L^{-1}. To evaluate the practical potential of an EC device, we increased the electrode loading level to ∼14 mg cm^{-2} (184 μm in thickness), which is similar to those of commercial electrodes. As shown in Figure 5c, the specific capacitance of CNG electrode with higher thickness was noted to be stable around 125 F g^{-1} at 1 A g^{-1}. Furthermore, the ESR increased slightly to 10 Ω. The performance of CNG electrode with a loading mass of 14 mg cm^{-2} is nearly as good as that of CNG with 2 mg cm^{-2} at low current densities and degrades only a little at high current densities (Figure S8a−c). Accordingly, the E_m and E_V were stable at 56 Wh kg^{-1} and 43 Wh L^{-1}, respectively (Figure S8d). These results demonstrate the loading mass of CNG materials in an EC device can be scaled up to obtain high energy for the entire cell. It is further highlighted that the high conductivity and excellent ion transport property of CNG enable high electrolyte-accessible surface area to ion adsorption and desorption and fast electron and ion transfer.

Moreover, the electrochemical performance against the entire configuration (including one separator, electrolyte, two current collectors, and two working electrodes) was also investigated. As shown in Table S1, the mass ratio of the active

electrode materials in a device without a package is about 76%. Accordingly, the CNG-based cell shows a maximum practical $E_{m-device}$ value of 43 Wh kg^{-1} and a highest $P_{m-device}$ value of 24 kW kg^{-1}. Correspondingly, the highest $E_{V-device}$ value and areal energy density (E_{area}) are about 34 Wh L^{-1} and 15.7 Wh m^{-2}, respectively, surpassing most previous results.[19,32,49,50,54] (Figure 5d). We attribute the high values to the synergistic action between the unique nanostructure and the doped heteroatom. First, the porous architecture in CNG forms a continuous porous channel for ion access of the interior surfaces of the electrode even with high thickness. Particularly, the void space distributed inside and between the wrinkled graphene sheets can function as ion-diffusion buffer. Additionally, the uniformly dispersed nitrogen groups on CNG can favor electrode and electrolyte interaction. Taken together, these advantages jointly enable CNG to obtain high gravimetric and volumetric capacities while retaining excellent rate performance.

■ EXPERIMENTAL SECTION

Materials Synthesis. CNG was prepared through a confined-polymerization and carbonization strategy. A total of 300 mg of MMT and 200 mg of dopamine (DA) were added into 200 mL of HCl solution (0.01 M) and agitated at room temperature for 1 day. Afterward, 10 mL of Tris buffer (0.1 M) was added dropwise and further stirred for more than 24 h. In the course of polymerization, the color of the aqueous solution gradually changed from white to black. The product of polymerization was collected by centrifugation and then further carbonized at 900 °C for 3 h in nitrogen. CNG was obtained by etching the MMT template by washing with 30% HF aqueous solution. For comparison, a nitrogen-free control sample GS prepared from phenolic resin with the same procedure.The reduced graphene oxide (rGO) was prepared through chemical reduction of graphene oxide (GO, prepared by modified Hummer method[55]) by NaBH$_4$. Typically, 2.0 g NaBH$_4$ was added into 100 mL of GO solution and stirred for 2 h. The rGO can be obtained after centrifuging and drying treatments.

Characterization. The structure and graphitization degree were analyzed by powder X-ray diffractions and Raman spectra, which were conducted on a Bruker D8 Advance X-ray diffractometer using Cu Kα radiation and HORIBA Scientific LabRAM HR Raman spectrometer system using a 532.4 nm laser, respectively. The morphology of CNG was analyzed by transmission electron microscopy and field-emission scanning electron microscopy, which were carried out with JEOL JEM-2010 and JEOL JSM-6380LV FESEM, respectively. The elemental composition was analyzed by X-ray photoelectron spectroscopy, which was recorded on a PerkinElmer PHI 550 spectrometer using Al Kα as the X-ray source. The porous structure of CNG was analyzed by N$_2$ sorption isotherms, which was performed on a Micromeritics BK122T-B analyzer. The SSA was calculated from the adsorption data within a relative pressure ranging from 0.04 to 0.2. The total pore volumes were estimated from the adsorbed amount at a relative pressure of 0.992. The Barrett−Joyner−Halenda (BJH) model was utilized for pore-size distribution calculations based on the adsorption branches of isotherms. An electrical conductivity test was completed on a SDY-5 four-point probe meter by using a conventional four-probe DC method. Packing density was determined simultaneously with electrical conductivity by employing a homemade apparatus under a load pressure of 8 MPa.

Electrochemical Measurements. The working electrodes for three-electrode system were prepared by mixing active material (5 mg), conductive additives, and polytetrafluorene−ethylene (PTFE) binder with a weight ratio of 80:15:5. The slurries was coated on the Ni foam (1 cm^2 × 1 cm^2) and then dried at 60 °C overnight. Prior to the electrochemical test, the electrode was pressed under 15 MPa. The symmetric supercapacitor was assembled as a 2016 type cell, using glass fiber (GF/D, Whatman) as the separator and 1-ethyl-3-

methylimidazolium tetrafluoroborate (EMImBF$_4$, > 98%) as electrolytes, respectively. The assembly process was carried out in an argon-filled glovebox. The working electrode was fabricated by mixing active material, conductive additives, and polyvinylidene fluoride (PVDF) binder with a weight ratio of 80:10:10 in N-methylpyrrolidinone (NMP) solvent. After being blended well, the mixture was rolled into a thin film and then punched into circular pellets. The pellet was then hot-pressed on the carbon-coated aluminum foil and dried at 110 °C overnight. All of the electrochemical measurements were carried out on a CHI 660D electrochemical workstation system (Chenhua, Shanghai). The EIS measurements were performed at open circuit potential with the 10^{-2} to 10^6 Hz frequency range at a 5 mV AC amplitude.

C_m was derived from galvanostatic discharge curve as

$$C_m = (I\Delta t)/(m\Delta V) \tag{1}$$

where Δt is the discharge time, Δs is the voltage variation (excluding the IR drop), I is the constant discharge current, and m is the mass of working electrodes. C_v was calculated by

$$C_v = C_m \times \rho \tag{2}$$

where ρ is the packing density of electrode material. The E_m and E_V of electrode materials and $E_{m-device}$ and $E_{V-device}$ of the entire EC device were evaluated on the basis of the following equations:

$$E_m = C_m V^2/2 \tag{3}$$

$$E_V = C_V V^2/2 \tag{4}$$

$$E_{m-device} = E_m \times M_m \tag{5}$$

$$E_{V-device} = E_V \times M_V \tag{6}$$

where V is the maximum voltage applied. M_m and M_V are the weight and volume percentage of active materials in the total device, respectively. The E_{area} of the entire device was evaluated on the basis of the following equation:

$$E_{area} = E_m \times M_{area} \tag{7}$$

where M_{area} is the mass per unit area of active materials in an EC device.

■ CONCLUSIONS

In conclusion, N-doped graphene with highly crumpled and hierarchical porous structure has been prepared as EC electrodes. The strategy presented here leads to graphene materials with highly conductive networks and fast ion diffusion paths. These unique features of CNG yield the formation of an efficient electric double layer over a highly ion-accessible surface, thus enabling a CNG electrode with outstanding gravimetric and volumetric performance in ionic liquid electrolyte. More importantly, the CNG-based EC devices are less independent of the loading level of the active material. Therefore, the as-prepared crumpled graphene with excellent gravimetric and volumetric performance exhibits promising potential for high-performance supercapacitors.

■ ASSOCIATED CONTENT

Ⓢ Supporting Information

The Supporting Information is available free of charge on the ACS Publications website at DOI: 10.1021/acsami.5b05428.

> Images showing the XRD patterns of the composite and NCG, SEM and schematic images of the structure of NCG, 1s XPS spectrum of NCG, TEM image of NCG and corresponding elemental mapping images for C and N, N$_2$ adsorption and desorption isotherms, contact-angle tests of GS and NCG, and images showing the

electrochemical performance of NCG. Table showing relevant experimental parameters. (PDF)

AUTHOR INFORMATION

Corresponding Author

*E-mail: azhangxg@163.com.

Notes

The authors declare no competing financial interest.

ACKNOWLEDGMENTS

REFERENCES

(1) Miller, J. R.; Simon, P. Electrochemical Capacitors for Energy Management. *Science* **2008**, *321*, 651−652.

(2) Simon, P.; Gogotsi, Y. Materials for Electrochemical Capacitors. *Nat. Mater.* **2008**, *7*, 845−854.

(3) Zhang, L. L.; Zhao, X. S. Carbon-Based Materials as Supercapacitor Electrodes. *Chem. Soc. Rev.* **2009**, *38*, 2520−2531.

(4) Simon, P.; Gogotsi, Y. Capacitive Energy Storage in Nano-structured Carbon−Electrolyte Systems. *Acc. Chem. Res.* **2013**, *46*, 1094−1103.

(5) You, B.; Jiang, J.; Fan, S. Three-Dimensional Hierarchically Porous All-Carbon Foams for Supercapacitor. *ACS Appl. Mater. Interfaces* **2014**, *6*, 15302−15308.

(6) Lu, X.; Zeng, Y.; Yu, M.; Zhai, T.; Liang, C.; Xie, S.; Balogun, M. S.; Tong, Y. Oxygen-Deficient Hematite Nanorods as High-Performance and Novel Negative Electrodes for Flexible Asymmetric Supercapacitors. *Adv. Mater.* **2014**, *26*, 3148−3155.

(7) Zhai, T.; Lu, X.; Ling, Y.; Yu, M.; Wang, G.; Liu, T.; Liang, C.; Tong, Y.; Li, Y. A New Benchmark Capacitance for Supercapacitor Anodes by Mixed-Valence Sulfur-Doped $V_6O_{13−x}$. *Adv. Mater.* **2014**, *26*, 5869−5875.

(8) Yao, Y.; Ma, C.; Wang, J.; Qiao, W.; Ling, L.; Long, D. Rational Design of High-Surface-Area Carbon Nanotube/Microporous Carbon Core-Shell Nanocomposites for Supercapacitor Electrodes. *ACS Appl. Mater. Interfaces* **2015**, *7*, 4817−4825.

(9) Shen, L.; Wang, J.; Xu, G.; Li, H.; Dou, H.; Zhang, X. $NiCo_2S_4$ Nanosheets Grown on Nitrogen-Doped Carbon Foams as an Advanced Electrode for Supercapacitors. *Adv. Energy Mater.* **2015**, *5*, 1400977.

(10) Wang, J.; Shen, L.; Nie, P.; Yun, X.; Xu, Y.; Dou, H.; Zhang, X. N-Doped Carbon Foam Based Three-Dimensional Electrode Architectures and Asymmetric Supercapacitors. *J. Mater. Chem. A* **2015**, *3*, 2853−2860.

(11) Zhao, J.; Chen, J.; Xu, S.; Shao, M.; Zhang, Q.; Wei, F.; Ma, J.; Wei, M.; Evans, D. G.; Duan, X. Hierarchical NiMn Layered Double Hydroxide/Carbon Nanotubes Architecture with Superb Energy Density for Flexible Supercapacitors. *Adv. Funct. Mater.* **2014**, *24*, 2938−2946.

(12) Rao, C. N. R.; Sood, A. K.; Subrahmanyam, K. S.; Govindaraj, A. Graphene: The New Two-Dimensional Nanomaterial. *Angew. Chem., Int. Ed.* **2009**, *48*, 7752−7777.

(13) Zhang, X.; Zhang, H.; Li, C.; Wang, K.; Sun, X.; Ma, Y. Recent Advances in Porous Graphene Materials for Supercapacitor Applications. *RSC Adv.* **2014**, *4*, 45862−45884.

(14) Zhu, J.; Yang, D.; Yin, Z.; Yan, Q.; Zhang, H. Graphene and Graphene-Based Materials for Energy Storage Applications. *Small* **2014**, *10*, 3480−3498.

(15) Low, C. T. J.; Walsh, F. C.; Chakrabarti, M. H.; Hashim, M. A.; Hussain, M. A. Electrochemical Approaches to The Production of Graphene Flakes and Their Potential Applications. *Carbon* **2013**, *54*, 1−21.

(16) El-Kady, M. F.; Strong, V.; Dubin, S.; Kaner, R. B. Laser Scribing of High-Performance and Flexible Graphene-Based Electrochemical Capacitors. *Science* **2012**, *335*, 1326−1330.

(17) Zhang, H.; Wang, K.; Zhang, X.; Lin, H.; Sun, X.; Li, C.; Ma, Y. Self-Generating Graphene and Porous Nanocarbon Composites for Capacitive Energy Storage. *J. Mater. Chem. A* **2015**, *3*, 11277−11286.

(18) Miller, J. R.; Outlaw, R. A.; Holloway, B. C. Graphene Double-Layer Capacitor with ac Line-Filtering Performance. *Science* **2010**, *329*, 1637−1639.

(19) Liu, C.; Yu, Z.; Neff, D.; Zhamu, A.; Jang, B. Z. Graphene-Based Supercapacitor with an Ultrahigh Energy Density. *Nano Lett.* **2010**, *10*, 4863−4868.

(20) Luo, J.; Jang, H. D.; Huang, J. Effect of Sheet Morphology on the Scalability of Graphene-Based Ultracapacitors. *ACS Nano* **2013**, *7*, 1464−1471.

(21) Wen, Z.; Wang, X.; Mao, S.; Bo, Z.; Kim, H.; Cui, S.; Lu, G.; Feng, X.; Chen, J. Crumpled Nitrogen-Doped Graphene Nanosheets with Ultrahigh Pore Volume for High-Performance Supercapacitor. *Adv. Mater.* **2012**, *24*, 5610−5616.

(22) Li, Y.; Li, Z.; Shen, P. K. Simultaneous Formation of Ultrahigh Surface Area and Three-Dimensional Hierarchical Porous Graphene-Like Networks for Fast and Highly Stable Supercapacitors. *Adv. Mater.* **2013**, *25*, 2474−2480.

(23) Wang, C.; Zhou, Y.; Sun, L.; Zhao, Q.; Zhang, X.; Wan, P.; Qiu, J. N/P-Codoped Thermally Reduced Graphene for High-Performance Supercapacitor Applications. *J. Phys. Chem. C* **2013**, *117*, 14912−14919.

(24) Lei, Z.; Lu, L.; Zhao, X. S. The Electrocapacitive Properties of Graphene Oxide Reduced by Urea. *Energy Environ. Sci.* **2012**, *5*, 6391−6399.

(25) Chen, P.; Yang, J. J.; Li, S. S.; Wang, Z.; Xiao, T. Y.; Qian, Y. H.; Yu, S. H. Hydrothermal Synthesis of Macroscopic Nitrogen-doped Graphene Hydrogels for Ultrafast Supercapacitor. *Nano Energy* **2013**, *2*, 249−256.

(26) Han, J.; Zhang, L. L.; Lee, S.; Oh, J.; Lee, K. S.; Potts, J. R.; Ji, J.; Zhao, X.; Ruoff, R. S.; Park, S. Generation of B-Doped Graphene Nanoplatelets Using a Solution Process and Their Supercapacitor Applications. *ACS Nano* **2013**, *7*, 19−26.

(27) Su, Y.; Zhang, Y.; Zhuang, X.; Li, S.; Wu, D.; Zhang, F.; Feng, X. Low-Temperature Synthesis of Nitrogen/Sulfur Co-Doped Three-Dimensional Graphene Frameworks as Efficient Metal-Free Electrocatalyst for Oxygen Reduction Reaction. *Carbon* **2013**, *62*, 296−301.

(28) Liang, J.; Jiao, Y.; Jaroniec, M.; Qiao, S. Z. Sulfur and Nitrogen Dual-Doped Mesoporous Graphene Electrocatalyst for Oxygen Reduction with Synergistically Enhanced Performance. *Angew. Chem., Int. Ed.* **2012**, *51*, 11496−11500.

(29) Cheng, Y.; Lu, S.; Zhang, H.; Varanasi, C. V.; Liu, J. Synergistic Effects from Graphene and Carbon Nanotubes Enable Flexible and Robust Electrodes for High-Performance Supercapacitors. *Nano Lett.* **2012**, *12*, 4206−4211.

(30) You, B.; Wang, L.; Li, N.; Zheng, C. Improving the Energy Storage Performance of Graphene through Insertion of Pristine CNTs and Ordered Mesoporous Carbon Coating. *ChemElectroChem* **2014**, *1*, 772−778.

(31) Gogotsi, Y.; Simon, P. True Performance Metrics in Electrochemical Energy Storage. *Science* **2011**, *334*, 917−918.

(32) Yang, X.; Cheng, C.; Wang, Y.; Qiu, L.; Li, D. Liquid-Mediated Dense Integration of Graphene Materials for Compact Capacitive Energy Storage. *Science* **2013**, *341*, 534−537.

(33) Yan, J.; Wang, Q.; Wei, T.; Jiang, L.; Zhang, M.; Jing, X.; Fan, Z. Template-Assisted Low Temperature Synthesis of Functionalized Graphene for Ultrahigh Volumetric Performance Supercapacitors. *ACS Nano* **2014**, *8*, 4720−4729.

(34) Tao, Y.; Xie, X.; Lv, W.; Tang, D. M.; Kong, D.; Huang, Z.; Nishihara, H.; Ishii, T.; Li, B.; Golberg, D.; Kang, F.; Kyotani, T.; Yang,

Q. H. Towards Ultrahigh Volumetric Capacitance: Graphene Derived Highly Dense But Porous Carbons for Supercapacitors. *Sci. Rep.* **2013**, *3*, 2975.

(35) Ling, Z.; Ren, C. E.; Zhao, M. Q.; Yang, J.; Giammarco, J. M.; Qiu, J.; Barsoum, M. W.; Gogotsi, Y. Flexible and Conductive MXene Films and Nanocomposites with High Capacitance. *Proc. Natl. Acad. Sci. U. S. A.* **2014**, *111*, 16676−16681.

(36) Ghidiu, M.; Lukatskaya, M. R.; Zhao, M. Q.; Gogotsi, Y.; Barsoum, M. W. Conductive Two-Dimensional Titanium Carbide/Clay/'with High Volumetric Capacitance. *Nature* **2014**, *516*, 78−81.

(37) Xu, Y.; Lin, Z.; Zhong, X.; Huang, X.; Weiss, N. O.; Huang, Y.; Duan, X. Holey Graphene Frameworks for Highly Efficient Capacitive Energy Storage. *Nat. Commun.* **2014**, *5*, 4554.

(38) Sonobe, N.; Kyotani, T.; Tomita, A. Formation of Graphite Thin Film from Polyfurfuryl Alcohol and Polyvinyl Acetate Carbons Prepared between the Lamellae of Montmorillonite. *Carbon* **1991**, *29*, 61−67.

(39) Ding, W.; Wei, Z.; Chen, S.; Qi, X.; Yang, T.; Hu, J.; Wang, D.; Wan, L. J.; Alvi, S. F.; Li, L. Space-Confinement-Induced Synthesis of Pyridinic- and Pyrrolic-Nitrogen-Doped Graphene for the Catalysis of Oxygen Reduction. *Angew. Chem., Int. Ed.* **2013**, *52*, 11755−11759.

(40) Fan, X.; Yu, C.; Yang, J.; Ling, Z.; Hu, C.; Zhang, M.; Qiu, J. A Layered-Nanospace-Confinement Strategy for the Synthesis of Two-Dimensional Porous Carbon Nanosheets for High-Rate Performance Supercapacitors. *Adv. Energy Mater.* **2015**, *5*, 5.

(41) Xu, Y.; Lin, Z.; Zhong, X.; Papandrea, B.; Huang, Y.; Duan, X. Solvated Graphene Frameworks as High-Performance Anodes for Lithium-Ion Batteries. *Angew. Chem.* **2015**, *127*, 5435−5440.

(42) Ding, J.; Wang, H.; Li, Z.; Kohandehghan, A.; Cui, K.; Xu, Z.; Zahiri, B.; Tan, X.; Lotfabad, E. M.; Olsen, B. C.; Mitlin, D. Carbon Nanosheet Frameworks Derived from Peat Moss as High Performance Sodium Ion Battery Anodes. *ACS Nano* **2013**, *7*, 11004−11015.

(43) Titirici, M. M.; Thomas, A.; Yu, S. H.; Müller, J. O.; Antonietti, M. A Direct Synthesis of Mesoporous Carbons with Bicontinuous Pore Morphology from Crude Plant Material by Hydrothermal Carbonization. *Chem. Mater.* **2007**, *19*, 4205−4212.

(44) Cui, C.; Qian, W.; Yu, Y.; Kong, C.; Yu, B.; Xiang, L.; Wei, F. Highly Electroconductive Mesoporous Graphene Nanofibers and Their Capacitance Performance at 4 V. *J. Am. Chem. Soc.* **2014**, *136*, 2256−2259.

(45) Kubo, S.; Tan, I.; White, R. J.; Antonietti, M.; Titirici, M. M. Template Synthesis of Carbonaceous Tubular Nanostructures with Tunable Surface Properties. *Chem. Mater.* **2010**, *22*, 6590−6597.

(46) You, B.; Yin, P.; An, L. Multifunctional Electroactive Heteroatom-Doped Carbon Aerogels. *Small* **2014**, *10*, 4352−4361.

(47) Zhang, J.; Chen, G.; Zhang, Q.; Kang, F.; You, B. Self-Assembly Synthesis of N-Doped Carbon Aerogels for Supercapacitor and Electrocatalytic Oxygen Reduction. *ACS Appl. Mater. Interfaces* **2015**, *7*, 12760−12766.

(48) Taberna, P. L.; Simon, P.; Fauvarque, J. F. Electrochemical Characteristics and Impedance Spectroscopy Studies of Carbon-Carbon Supercapacitors. *J. Electrochem. Soc.* **2003**, *150*, A292−A300.

(49) Burke, A. R& D Considerations for The Performance and Application of Electrochemical Capacitors. *Electrochim. Acta* **2007**, *53*, 1083−1091.

(50) Izadi-Najafabadi, A.; Yasuda, S.; Kobashi, K.; Yamada, T.; Futaba, D. N.; Hatori, H.; Yumura, M.; Iijima, S.; Hata, K. Extracting the Full Potential of Single-Walled Carbon Nanotubes as Durable Supercapacitor Electrodes Operable at 4 V with High Power and Energy Density. *Adv. Mater.* **2010**, *22*, E235−E241.

(51) Hao, G. P.; Lu, A. H.; Dong, W.; Jin, Z. Y.; Zhang, X. Q.; Zhang, J. T.; Li, W. C. Sandwich-Type Microporous Carbon Nanosheets for Enhanced Supercapacitor Performance. *Adv. Energy Mater.* **2013**, *3*, 1421−1427.

(52) Sevilla, M.; Fuertes, A. B. Direct Synthesis of Highly Porous Interconnected Carbon Nanosheets and Their Application as High-Performance Supercapacitors. *ACS Nano* **2014**, *8*, 5069−5078.

(53) Kim, T.; Jung, G.; Yoo, S.; Suh, K. S.; Ruoff, R. S. Activated Graphene-Based Carbons as Supercapacitor Electrodes with Macro- and Mesopores. *ACS Nano* **2013**, *7*, 6899−6905.

(54) Zhu, Y.; Murali, S.; Stoller, M. D.; Ganesh, K. J.; Cai, W.; Ferreira, P. J.; Pirkle, A.; Wallace, R. M.; Cychosz, K. A.; Thommes, M.; Su, D.; Stach, E. A.; Ruoff, R. S. Carbon-Based Supercapacitors Produced by Activation of Graphene. *Science* **2011**, *332*, 1537−1541.

(55) Hummers, W. S.; Offeman, R. E. Preparation of Graphitic Oxide. *J. Am. Chem. Soc.* **1958**, *80*, 1339−1339.